Resonance Raman Intensity Analysis of Excited-State Dynamics

ANNE B. MYERS

Department of Chemistry, University of Rochester, Rochester, New York 14627−0216

Received May 18, 1997

Introduction

To a chemist, the geometry of a molecule is one of its defining properties. The equilibrium structure of a stable molecule in its ground electronic state can often be determined quite accurately through diffraction techniques and/or a variety of spectroscopic probes. Excited electronic states present a greater challenge since their comparatively short lifetimes preclude the application of many of these techniques. The classic experimental method for determining excited-state geometries involves analysis of line positions in high-resolution absorption or emission spectra. This method has the significant limitation of requiring sharp spectral lines, eliminating the possibility of examining arbitrary environmental perturbations on the molecular structure. Furthermore, many electronic spectra are *intrinsically* broad due to fast photochemical or photophysical dynamics. One might argue that the "structure" of a very short-lived state is not even meaningful. However, within the Born−Oppenheimer approximation, there still exist one or more potential energy surfaces on which these fast processes occur, and these surfaces are no less interesting when they are unbound or weakly bound, or undergo crossings or near-crossings with other surfaces.

When direct electronic spectroscopies are of limited utility, the next best experimental approach is to employ a higher-order spectroscopy that uses the excited electronic state of interest as an intermediate state. Since the transition line width depends only on the initial and final states, multiphoton spectroscopies provide a way to circumvent the "uncertainty principle" broadening of short-lived electronic states. Resonance Raman is a particularly useful higher-order spectroscopy since both initial and final levels belong to the ground electronic state, which is generally long-lived (yielding sharp vibrational transitions) and often well-characterized spectroscopically. Spontaneous Raman signals are linear in the incident intensity, but two photons are involved, one being spontaneously generated. In the traditional view of Raman scattering, a net vibrational transition is achieved through "virtual" excitation and deexcitation of higher energy states. As the incident light is tuned toward resonance with a particular electronic state, its vibrational levels dominate the scattering process, and the *resonance* Raman intensities reflect the properties of that state.

The vibronic theory of resonance Raman was developed in detail in the 1960s and 1970s.[1−3] It was established that for resonance with strongly allowed transitions the dominant Raman lines involve totally symmetric vibrations that are Franck−Condon active in the electronic transition and that modeling of excitation profiles and intensities could therefore be used to deduce geometry changes accompanying electronic excitation. However, application of the theory was largely stymied by the severe computational requirements for complex molecules, even when assuming simple harmonic models for the potential surfaces. The sum-over-states formalism is particularly unenlightening for resonance with dissociative surfaces supporting no bound vibrational states, and provides little insight into the relationship between resonance Raman intensities and excited-state dynamics. That changed with the introduction of the time-dependent wave packet picture of Raman scattering by Heller and co-workers in 1979.[4,5] This formulation brings out the relationship between excited-state properties and steady-state resonance Raman intensities in a way that highlights the utility of the technique for exploring dynamics of short-lived electronic states.

This Account summarizes the theory of resonance Raman intensities, with emphasis on time−domain approaches and modifications needed to treat processes occurring in condensed phases. It then presents a few representative examples, drawn from my group's work, of applications of the theory to experimental data. Recent reviews of other subfields within this broad topic can be found in refs 6−11.

Theory

In a Raman process, the total scattered power $P_{i\rightarrow f}$ (photons s^{-1}) arising from a particular initial to final vibrational state transition, integrated over the Raman line width and over all polarization and propagation directions for the scattered light, is given by

$$P_{i\rightarrow f} = I_L N_i \sigma_{R,i\rightarrow f} \qquad (1)$$

where I_L is the laser intensity, N_i is the number of

Anne B. Myers was born May 9, 1958 in New Haven, Connecticut, but grew up and was educated in California (B.S. in chemistry, UC Riverside, 1980; Ph.D. with Rich Mathies in biophysical chemistry, UC Berkeley, 1984). Shen then moved east to spend 2 years as an NIH post-doctoral fellow with Robin Hochstrasser at the University of Pennsylvania and in 1987 joined the faculty at the University of Rochester, where she is now professor of chemistry. She has twice received visiting fellowships to investigate new problems in other environments (IBM Almaden in 1992−93 and JILA in 1997−98). Her research interests include theoretical and experimental resonance Raman spectroscopy, ultrafast molecular dynamics in condensed phases, photoinduced electron transfer, single molecule spectroscopy, and nonlinear optics.

(1) Albrecht, A. C.; Hutley, M. C. *J. Chem. Phys.* **1971**, *55*, 4438−4443.
(2) Johnson, B. B.; Peticolas, W. L. *Ann. Rev. Phys. Chem.* **1976**, *27*, 465−491.
(3) Warshel, A.; Dauber, P. *J. Chem. Phys.* **1977**, *66*, 5477−5488.
(4) Lee, S.-Y.; Heller, E. J. *J. Chem. Phys.* **1979**, *71*, 4777−4787.
(5) Heller, E. J. *Acc. Chem. Res.* **1981**, *14*, 368−375.
(6) Myers, A. B. *Chem. Rev.* **1996**, *96*, 911−926.
(7) Johnson, B. R.; Kittrell, C.; Kelly, P. B.; Kinsey, J. L. *J. Phys. Chem.* **1996**, *100*, 7743−7764.
(8) Myers, A. B. In *Laser Techniques in Chemistry*; Myers, A. B., Rizzo, T. R., Eds.; Wiley: New York, 1995; pp 325−384.
(9) Ziegler, L. D. *Acc. Chem. Res.* **1994**, *27*, 1−8.
(10) Asher, S. A. *Anal. Chem.* **1993**, *65*, 59−66.
(11) Zink, J. I.; Shin, K.-S. K. *Adv. Photochem.* **1991**, *16*, 119−214.

S0001-4842(96)00240-3 CCC: $14.00

scatterers in state $|i\rangle$ within the illuminated volume, and $\sigma_{R,i\to f}$ is the Raman cross section. Most experimental geometries actually detect scattering into a range of solid angles Ω about a particular direction, which is proportional to the differential cross section, $(d\sigma/d\Omega)_{R,i\to f}$. The relationship between σ and $(d\sigma/d\Omega)$ depends on the scattering geometry and the Raman depolarization ratio.[12]

The usual formulation of vibrational Raman scattering assumes an isolated molecule interacting with weakly perturbing incident monochromatic radiation. The molecule starts in a vibrational state of the ground electronic surface, $|i\rangle$, and time-dependent perturbation theory is used to calculate the rate of change, in the steady-state limit, of the probability for finding the molecule in a different vibrational state $|f\rangle$ following one interaction with the incident and one with the scattered field. The perturbed wavefunction resulting from each radiation-matter interaction is expanded in the stationary eigenfunctions of the molecular Hamiltonian, resulting in a summation over all "paths" $|i\rangle \to \{|v\rangle\} \to |f\rangle$ where $|v\rangle$ represents any state that is transition dipole coupled to both $|i\rangle$ and $|f\rangle$. For resonance Raman it is usually assumed that only vibrational levels of the resonant electronic state contribute significantly as intermediate states, and the cross section becomes

$$\sigma_{R,i\to f}(E_L) = \frac{8\pi e^4 M^4 E_L E_S^3}{9\hbar^4 c^4} \left| \sum_v \frac{\langle f|v\rangle\langle v|i\rangle}{\epsilon_v + E_0 - \epsilon_i - E_L - i\hbar\gamma/2} \right|^2 \quad (2)$$

Here, E_L and E_S are the incident and scattered photon energies, ϵ_v and ϵ_i are the vibrational energies of the intermediate and initial states, E_0 is the electronic zero−zero energy, M is the electronic transition length (assumed independent of nuclear coordinates), and γ is the inverse electronic lifetime (assumed independent of vibrational level). For polyatomic molecules, each vibrational overlap is $(3N - 6)$-dimensional, although these are often approximated as products of one-dimensional overlaps:

$$\langle v|i\rangle = \langle v|i\rangle_1 \langle v|i\rangle_2 \langle v|i\rangle_3 \ldots \langle v|i\rangle_{3N-6} \quad (3)$$

The optical absorption cross section at the same level of theory is given by

$$\sigma_{i,A}(E_L) = \frac{4\pi e^2 M^2 E_L}{3\hbar c} \sum_v \frac{(\hbar\gamma/2)|\langle v|i\rangle|^2}{(\epsilon_v + E_0 - \epsilon_i - E_L)^2 + (\hbar\gamma/2)^2} \quad (4)$$

a sum over all vibronic transitions each clothed by a normalized Lorentzian line shape and weighted by its Franck−Condon factor, $|\langle v|i\rangle|^2$.

Equations 2 and 4, together with Figure 1, bring out some essential similarities between optical absorption spectra and resonance Raman intensities. For a mode to have intensity in the resonance Raman, there must be some intermediate state(s) $|v\rangle$ that have good overlaps with both $|i\rangle$ and $|f\rangle$, which can occur only if the potential surface for the resonant state has a different frequency and/or potential minimum from that of the ground state along that coordinate. This is the same requirement for the Franck−Condon factors $|\langle v|i\rangle|^2$ to be nonzero and, thus, for that mode's frequency to appear in a vibrationally resolved absorption spectrum.

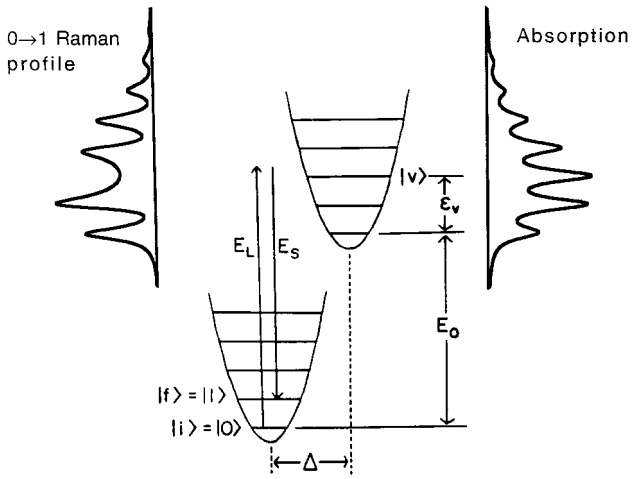

FIGURE 1. One-dimensional picture of sum-over-states formulation of absorption and resonance Raman.

Computational evaluation of eq 2 can be unreasonably time-consuming because of the number of levels $|v\rangle$ that must be considered for large molecules or those with dissociative excited states. The problem can be made somewhat tractable by assuming separability of the vibrations as in eq 3 and by assuming that the vibrations are harmonic, although these are often poor approximations. Each individual overlap integral is then easy to calculate, but the total number of terms in the sum may still be enormous. In addition, a single $\sigma_{i\to f}$ is rarely measured directly, since many near-degenerate $|i\rangle \to |f\rangle$ transitions can contribute to scattering at a given frequency. Finally, eq 2 is correct only if the "chromophore" (the part of the system of which $|i\rangle$, $|v\rangle$, and $|f\rangle$ are eigenstates) is in a quantum mechanical pure state; that is, it is not interacting significantly with any extrachromophoric material degrees of freedom.

All of these difficulties may be mitigated by starting from a density matrix formulation and performing the calculations in the time domain.[13,14] For excitation on resonance with a single electronic state in the Condon approximation, the rate of detecting emitted photons at frequency ω_S, assuming monochromatic incident radiation of frequency ω_L, is[14]

$$\sigma_{SLE}(\omega_L,\omega_S) = \frac{4\omega_L\omega_S^3 M^4 e^4}{9\hbar^2 c^4} S_{SLE}(\omega_L,\omega_S) \quad (5)$$

where

$$S_{SLE}(\omega_L,\omega_S) = 2\,\mathrm{Re}\int_0^\infty dt_3 \int_0^\infty dt_2 \int_0^\infty dt_1 \{\exp(i\omega_L t_1 + i\omega_S t_3)\, R_1(t_3,t_2,t_1) + \exp(-i\omega_L t_1 + i\omega_S t_3)\, R_2(t_3,t_2,t_1) + \exp[-i\omega_L t_1 - i(\omega_L - \omega_S)t_2 + i\omega_S t_3]\, R_3(t_3,t_2,t_1)\} \quad (6)$$

and

(12) Nafie, L.; Stein, P.; Fanconi, B.; Peticolas, W. L. *J. Chem. Phys.* **1970**, *52*, 1584−1588.
(13) Sue, J.; Yan, Y. J.; Mukamel, S. *J. Chem. Phys.* **1986**, *85*, 462−474.
(14) Mukamel, S. *Principles of Nonlinear Optical Spectroscopy*; Oxford University Press: New York, 1995.

$$R_1(t_3,t_2,t_1) = \exp[-i\omega_0(t_3 + t_1) - (\gamma/2)(t_3 + t_1) - \gamma t_2] \times \exp[-g^*(t_3) - g(t_1) - f_+(t_3,t_2,t_1)] \quad (7a)$$

$$R_2(t_3,t_2,t_1) = \exp[-i\omega_0(t_3 - t_1) - (\gamma/2)(t_3 + t_1) - \gamma t_2] \times \exp[-g^*(t_3) - g^*(t_1) + f_+^*(t_3,t_2,t_1)] \quad (7b)$$

$$R_3(t_3,t_2,t_1) = \exp[-i\omega_0(t_3 - t_1) - (\gamma/2)(t_3 + t_1)] \times \exp[-g(t_3) - g^*(t_1) + f_-^*(t_3,t_2,t_1)] \quad (7c)$$

$$f_-(t_3,t_2,t_1) = g(t_2) - g(t_2 + t_3) - g(t_1 + t_2) + g(t_1 + t_2 + t_3) \quad (7d)$$

$$f_+(t_3,t_2,t_1) = g^*(t_2) - g^*(t_2 + t_3) - g(t_1 + t_2) + g(t_1 + t_2 + t_3) \quad (7e)$$

where $\omega_0 = E_0/\hbar$. The quantity $g(t)$ contains all information about the nuclear dynamics

$$g(t) = g_{vib}(t) + g_{solv}(t) \quad (8)$$

where $g_{vib}(t)$ is the contribution from the relatively high-frequency intramolecular vibrations of the chromophore and $g_{solv}(t)$ accounts for all low-frequency (or static) solvent or intermolecular modes that contribute to "pure dephasing" and/or "inhomogeneous broadening", depending on the time scale.

Equation 6 imposes no artificial distinction between "Raman" and "fluorescence" and assumes no separation of time scales among the various processes that contribute to $g(t)$. If there is no environment or the solvent contributes only to an exponential pure dephasing, and a single vibrational ground state is initially populated, then the three-time integral in eq 6 may be rewritten as the modulus squared of a one-time integral[13,15]

$$S_{SLE}(\omega_L,\omega_S) = S_{Raman}(\omega_L,\omega_S) + S_{Fluor}(\omega_L,\omega_S) \quad (9)$$

where

$$S_{Raman}(\omega_L,\omega_S) \propto M^4\omega_L\omega_S^3 \sum_f \left| \int_0^\infty dt\, \langle f|i(t)\rangle \exp[i(\omega_L + \omega_i - \omega_0)t - g_{solv}(t) - \gamma t/2] \right|^2 \delta(\omega_L - \omega_S - \omega_{fi}) \quad (10)$$

and $S_{Fluor}(\omega_L,\omega_S)$ describes a usually much broader emission that underlies the sharp Raman spectrum. The quantity $|i(t)\rangle = \exp(-iH_{ex}t/\hbar)\,|i\rangle$ is the initial vibrational wave function propagated by the excited-state vibrational Hamilitonian, and the time-dependent overlap $\langle f|i(t)\rangle$ is what becomes of $g_{vib}(t)$ from eq 8. While the δ function is often replaced by some other function representing a realistic ground-state vibrational line shape, the separation that leads to eq 10 is rigorously correct only in the limit of vanishing vibrational line widths.[16]

Equation 10 is essentially Heller's time-dependent formulation of resonance Raman scattering[4,17,18] (Figure 2). The demonstration that the Raman amplitude could be expressed as the half-Fourier-transform of a time-dependent overlap, requiring no explicit summation over vibronic eigenstates, was a tremendous advance. It made calculations on large molecules routinely feasible for the first time, as the computational effort in calculating and Fourier transforming the multidimensional overlaps in eq 10, at least for separable dynamics, is far less than that required to sum over all possible intermediate states in eq 2. It also facilitated calculations on dissociative potentials by emphasizing that such spectra are determined by only the *initial* motion of $|i(t)\rangle$ and thus require the excited-state surface only in the region near the ground-state geometry.

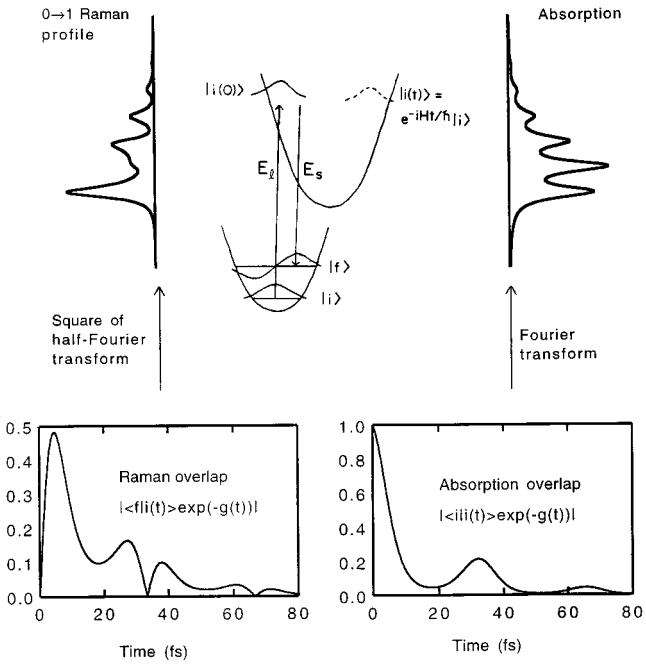

FIGURE 2. One-dimensional picture of time-domain formulation of absorption and resonance Raman.

Heller's derivation assumed isolated molecules and pure lifetime broadening. By starting with eq 6, one can show that a result such as eq 10 is more general and holds approximately in the presence of an environment, provided the dynamics described by $g_{solv}(t)$ are fast compared with the inverse ground-state vibrational line width.[13] Static ("inhomogeneous") contributions to $g_{solv}(t)$ may also be incorporated by averaging the entire cross section over a distribution of electronic transition energies and/or other parameters. A Boltzmann distribution of initial vibrational states is handled similarly. The distinction is that "homogeneous" broadening *on the Raman time scale* affects the resonance Raman *amplitude*, while "inhomogeneous" broadening contributes to a distribution of *cross sections*.[19]

Stochastic models for the solvent−solute coupling assume that the energy levels of the chromophore fluctuate about some fixed mean due to random forces exerted by the environment.[13,15,20,21] These models can describe the evolution of the electronic line shape from "inhomogeneous" (Gaussian) to "homogeneous" (Lorentzian) as

(15) Mukamel, S. *J. Chem. Phys.* **1985**, *82*, 5398−5408.
(16) Lee, D.; Albrecht, A. C. *Adv. Infrared Raman Spectrosc.* **1985**, *12*, 179−213.
(17) Heller, E. J.; Sundberg, R. L.; Tannor, D. *J. Phys. Chem.* **1982**, *86*, 1822−1833.
(18) Myers, A. B.; Mathies, R. A.; Tannor, D. J.; Heller, E. J. *J. Chem. Phys.* **1982**, *77*, 3857−3866.
(19) Myers, A. B.; Mathies, R. A. In *Biological Applications of Raman Spectroscopy*; Spiro, T. G., Ed.; Wiley: New York, 1987; Vol. 2, pp 1−58.
(20) Kubo, R. *Solid State Commun.* **1979**, *32*, 1−6.
(21) Takagahara, T.; Hanamura, E.; Kubo, R. *J. Phys. Soc. Jpn.* **1977**, *43*, 802−810.

the fluctuation rate increases. They are, however, incomplete in that they consider the effect of the solvent on the solute, but not vice versa. A model that overcomes these shortcomings with little additional complexity is the Brownian oscillator,[14,22] which treats the nuclear motions as one or more harmonic vibrations each characterized by a frequency (identical in ground and excited states), a ground- to excited-state displacement, and a frictional damping. The friction can be varied continuously from zero (typically used for high-frequency intramolecular vibrations) to strongly overdamped (for collective solvation modes). For strongly overdamped modes in the high temperature limit, $g_{solv}(t)$ becomes

$$g_{solv}(t) = (2\lambda k_B T/\hbar\Lambda^2)[\exp(-\Lambda t) + \Lambda t - 1] - i(\lambda/\Lambda)[\exp(-\Lambda t) + \Lambda t - 1] \quad (11)$$

where λ is the Stokes shift and Λ is the inverse time scale, related to the frequency of the oscillator and the friction. The real part of $g_{solv}(t)$ generates broadening of the chromophore's vibronic transitions that can vary from Lorentzian to Gaussian depending on the relative magnitudes of Λ and λ, while the imaginary part gives the Stokes shift between absorption and fluorescence. More general formulas for the Brownian oscillator are given in refs 14, 22, and 23.

Applications

Predissociative Triatomic Molecules. The strong, far-UV $S_3 \leftrightarrow S_0$ transitions of CS_2 and SO_2 are good test cases for Raman intensity analysis. Their gas-phase absorption spectra show vibrational resolution and some rotational structure near the origin, but at higher energies the lines are broadened by predissociation. In solution the absorption spectra are almost completely diffuse. The principal difficulty with simulating the spectra is that the geometry changes between S_0 and S_3 are large and cannot be well represented by simple separable harmonic oscillators.

We modeled CS_2 as separable harmonic symmetric and antisymmetric stretches (ν_1 and ν_3) and a two-dimensional anharmonic bend (ν_2).[24] The calculations were carried out using the sum over vibronic states approach of eqs 2−4 with electronic inhomogeneous broadening included. The excited-state potential parameters were constrained to give the S_3 equilibrium geometry obtained from partial rotational analysis of the gas-phase absorption and to approximately reproduce the vibronic spacings in the jet-cooled absorption spectrum and were refined within these constraints to best reproduce the observed solution phase spectra. Both the absorption spectrum and the absolute resonance Raman intensities were reasonably well reproduced by this simple model. The inhomogeneous broadening merely redistributes the intensity in both the absorption spectrum and the Raman excitation profiles without affecting the profile-integrated Raman intensities, while the homogeneous broadening also damps the Raman cross sections. Therefore, the absolute cross sections allow the two contributions to the breadth to be separated. Figure 3 compares the experimental and calculated spectra.

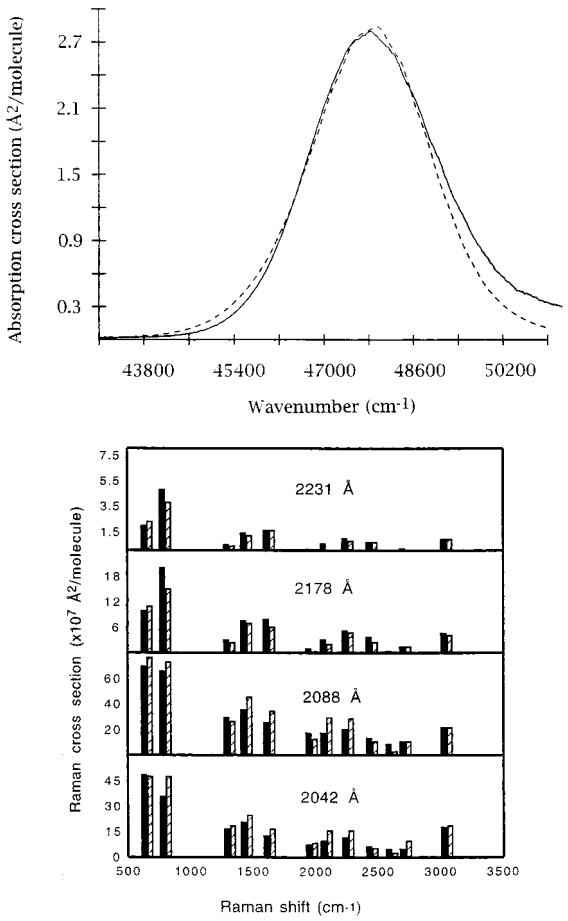

FIGURE 3. Comparison of experimental (solid) and calculated (dashed and striped) $S_3 \leftrightarrow S_0$ absorption spectra and resonance Raman intensities of CS_2 in cyclohexane. Parameters of the calculations are given in ref 24.

For SO_2, we utilized an anharmonic potential energy surface for the S_3 state previously developed to fit vibronic energy levels of the isolated molecule.[25] This surface includes coupling between the symmetric and antisymmetric stretches to produce a global potential minimum at a geometry having unequal S−O bond lengths. The calculations were carried out using the time−domain expression of eq 10, with $|i(t)\rangle$ calculated via numerical wave packet propagation on this two-dimensional anharmonic surface using the methods of Feit and Fleck.[26] The good agreement between calculated and experimental resonance Raman intensities shown in Figure 4 suggests that the potential surfaces change little between the vapor phase and hexane solution.

Excited States of Linear Polyenes: Solvent Effects. The lowest allowed electronic transitions of small polyenes are rather diffuse even in cold isolated molecules and are strongly red-shifted in solution relative to the vapor. Resonance Raman spectroscopy has been helpful in revealing the vibronic structure that underlies these diffuse transitions and examining solvent effects on the potential surfaces.

The room-temperature vapor phase absorption spectrum of *trans*-1,3,5-hexatriene exhibits modest vibrational

(22) Gu, Y.; Champion, P. M. *Chem. Phys. Lett.* **1990**, *171*, 254−258.
(23) Li, B.; Johnson, A. E.; Mukamel, S.; Myers, A. B. *J. Am. Chem. Soc.* **1994**, *116*, 11039−11047.
(24) Myers, A. B.; Li, B.; Ci, X. *J. Chem. Phys.* **1988**, *89*, 1876−1886.
(25) Yang, T.-S.; Myers, A. B. *J. Chem. Phys.* **1991**, *95*, 6207−6217.
(26) Feit, M. D.; Fleck, J. A., Jr. *J. Chem. Phys.* **1983**, *78*, 301−308.

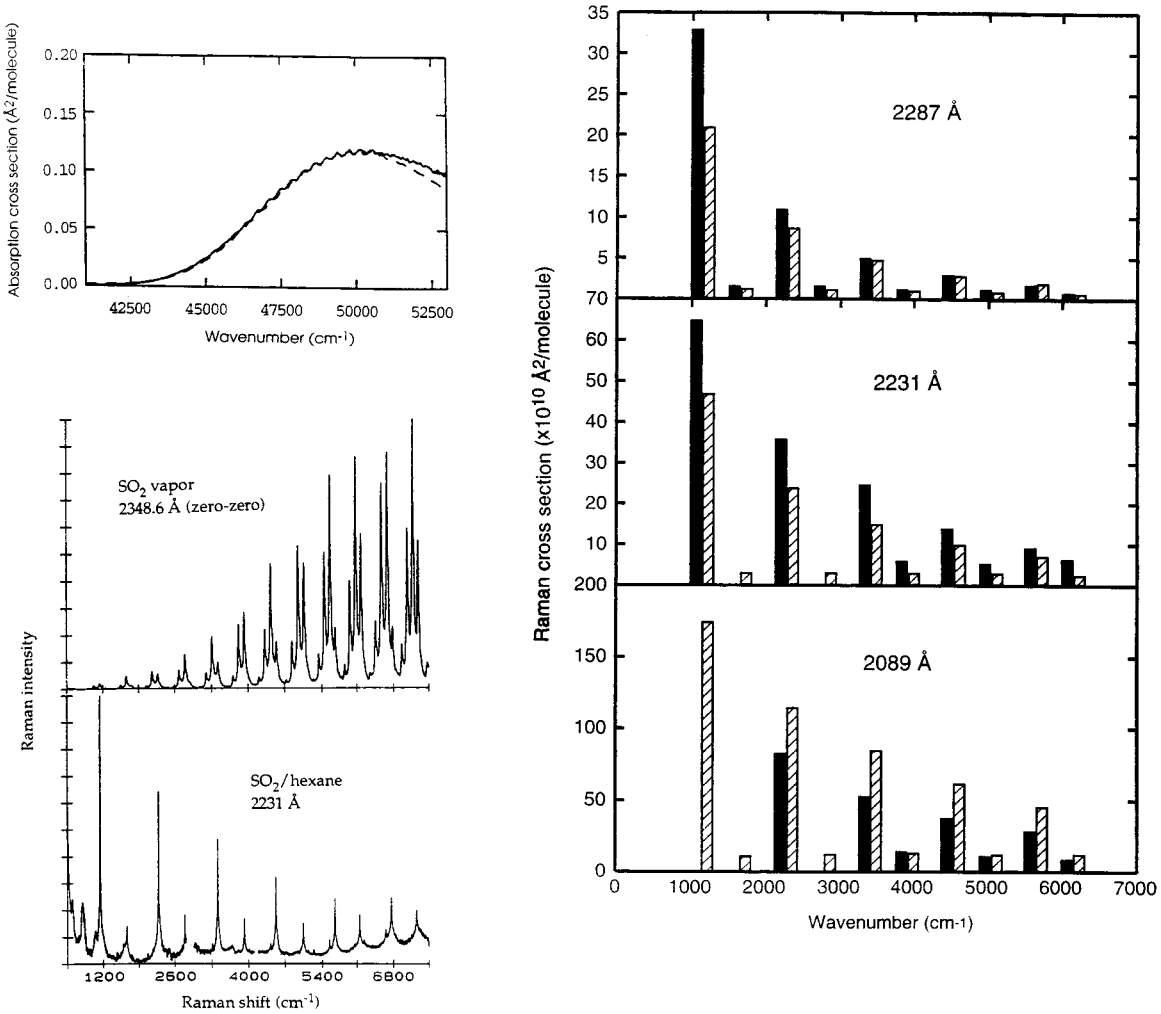

FIGURE 4. Comparison of experimental (solid) and calculated (dashed and striped) $S_3 \leftrightarrow S_0$ absorption spectra and resonance Raman intensities of SO_2 in hexane using vapor phase potential surface parameters with additional solvent-induced homogeneous broadening. Parameters of the calculations are given in ref 25. The vapor and solution phase resonance Raman/resonance fluorescence spectra are also shown for comparison.

structure, and the relative Raman intensities vary strongly with excitation frequency. The sensitivity of both the absorption spectral structure and the Raman profiles to the potential parameters allows determination of the excited-state potential surface in some detail.[27,28] Solvation broadens the absorption spectrum and greatly reduces the intensity in overtones of the low-frequency out-of-plane modes.[29] As the solvent polarizability is increased, there is a strong correlation between the red-shift of the absorption spectrum and further reductions in torsional resonance Raman intensities (Figure 5). Some of this is attributable to the faster electronic dephasing in solution, which preferentially reduces the Raman cross sections of low-frequency modes and/or overtones because these require a longer time to reach the first maximum in $\langle f|i(t)\rangle$.[19,30] However, this effect accounts for only part of the observed intensity changes, leading to the conclusion that the frequency change upon electronic excitation (presumably a frequency *decrease* for predominantly double bond torsions) becomes less pronounced in solution; that is, increasing the solvent polarizability causes a stiffening of the excited-state potential surface for double-bond torsion. Similar but less dramatic solvent effects were observed in *cis*-1,3,5-hexatriene[31] and 1,3-butadiene.[32]

None of these small polyenes exhibit significant relaxed fluorescence, even compared with the weak Raman scattering. This implies that the homogeneous broadening producing the relatively unstructured vapor phase absorption spectra should be attributed mainly to sub-100 fs depopulation of the optically allowed state, although the non-Lorentzian line shapes indicate that this decay is substantially nonexponential in time. It may arise from surface crossing to an optically forbidden electronic state that occurs some distance from the Franck–Condon region.[33,34]

Reorganization Energies in Photoinduced Charge Transfer. There are special reasons for interest in the vibrational Franck–Condon factors for systems in which electronic excitation corresponds to formal electron transfer from a neutral ground state, DA, to an ion-pair excited

(27) Myers, A. B.; Pranata, K. S. *J. Phys. Chem.* **1989**, *93*, 5079–5087.
(28) Torii, H.; Tasumi, M. *J. Chem. Phys.* **1994**, *101*, 4496–4504.
(29) Ci, X.; Pereira, M. A.; Myers, A. B. *J. Chem. Phys.* **1990**, *92*, 4708–4717.
(30) Myers, A. B.; Mathies, R. A. *J. Chem. Phys.* **1984**, *81*, 1552–1558.
(31) Ci, X.; Myers, A. B. *J. Chem. Phys.* **1992**, *96*, 6433–6442.
(32) Phillips, D. L.; Zgierski, M. Z.; Myers, A. B. *J. Phys. Chem.* **1993**, *97*, 1800–1809.
(33) Celani, P.; Garavelli, M.; Ottani, S.; Bernardi, F.; Robb, M. A.; Olivucci, M. *J. Am. Chem. Soc.* **1995**, *117*, 11584–11585.
(34) Orlandi, G.; Zerbetto, F.; Zgierski, M. Z. *Chem. Rev.* **1991**, *91*, 867–891.

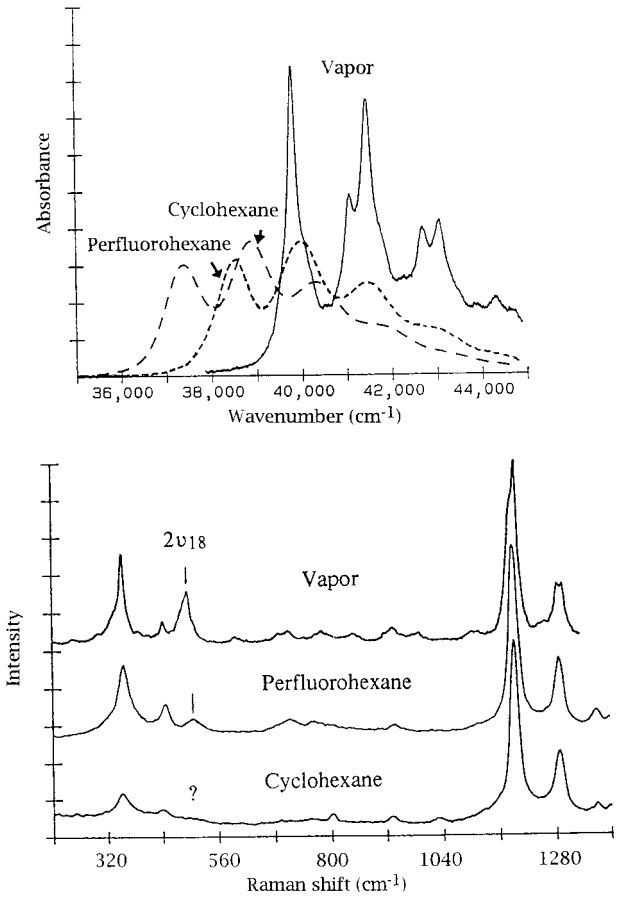

FIGURE 5. Absorption and resonance Raman spectra of *trans*-1,3,5-hexatriene in vapor phase, perfluorohexane, and cyclohexane solution; $2\nu_{18}$ is the double-bond torsional overtone.

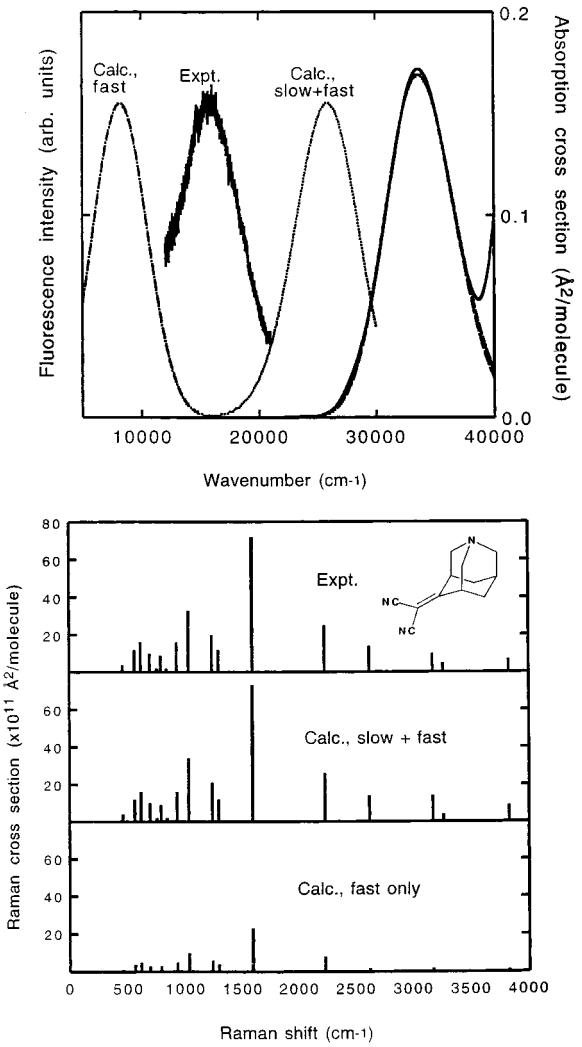

FIGURE 6. Absorption and fluorescence spectra and 310 nm excited resonance Raman intensities of a covalent charge-transfer azaadamantane. The "slow + fast" calculations, which best fit the experimental Raman intensities but underestimate the fluorescence Stokes shift (parameters of ref 41), assume that most of the solvent-induced broadening is static on the experimental time scale; the "fast only" calculations assume no static component and overestimate the Stokes shift while underestimating the Raman cross sections. The zero−zero energies are chosen to superimpose the calculated absorption spectra.

state, $D^{\bullet+}/A^{\bullet-}$.[6,35−38] The decay of the ion-pair state by radiationless return electron transfer is usually described by a Golden Rule rate written as the product of an electronic coupling and a vibrational Franck−Condon factor which depends on the frequencies and geometry changes along all of the coupled vibrations. Resonance Raman intensity analysis provides, in principle, a way to determine the vibrational part of the return electron transfer rate, usually expressed as the contribution from each mode to the "reorganization energy".

Our initial studies focused on the noncovalent hexamethylbenzene/tetracyanoethylene charge-transfer complex. We simultaneously modeled the absorption and fluorescence spectra and the absolute Raman excitation profiles for 11 vibrations to obtain the mode-specific reorganization energies.[39] The contribution of the solvent to the electronic spectral broadening and the Stokes shift was incorporated by using the Brownian oscillator model. While the fits to the data were generally good, the solvent reorganization energy of 2450 cm^{-1} seemed unphysically large for a nonpolar solvent (CCl_4). The "solvent" reorganization may include large geometry changes between the neutral and ion-pair states along intermolecular coordinates that are too low in frequency to be observed directly in the resonance Raman spectrum.

Complications arising from multiple ground-state conformers and/or complex stoichiometries and low-frequency anharmonic intermolecular modes are absent in covalent donor−acceptor molecules such as the substituted adamantane in Figure 6. At least 13 vibrational fundamentals coupled to the charge-transfer transition have been tentatively assigned.[40] In methanol solvent, successful modeling of the absorption spectrum and the absolute resonance Raman intensities required a fairly large contribution from solvent-induced broadening that is inhomogeneous on the Raman time scale.[41] Interestingly, comparison of calculated and observed fluorescence

(35) Doorn, S. K.; Hupp, J. T. *J. Am. Chem. Soc.* **1989**, *111*, 1142−1144.
(36) Buhks, E.; Bixon, M.; Jortner, J.; Navon, G. *J. Phys. Chem.* **1981**, *85*, 3759−3762.
(37) Barbara, P. F.; Meyer, T. J.; Ratner, M. A. *J. Phys. Chem.* **1996**, *100*, 13148−13168.
(38) Barqawi, K. R.; Murtaza, Z.; Meyer, T. J. *J. Phys. Chem.* **1991**, *95*, 47−50.
(39) Kulinowski, K.; Gould, I. R.; Myers, A. B. *J. Phys. Chem.* **1995**, *99*, 9017−9026.
(40) Lilichenko, M.; Verhoeven, J. W.; Myers, A. B. *Spectrochim. Acta* In press.
(41) Phillips, D. L.; Gould, I. R.; Verhoeven, J. W.; Tittelbach-Helmrich, D.; Myers, A. B. *Chem. Phys. Lett.* **1996**, *258*, 87−93.

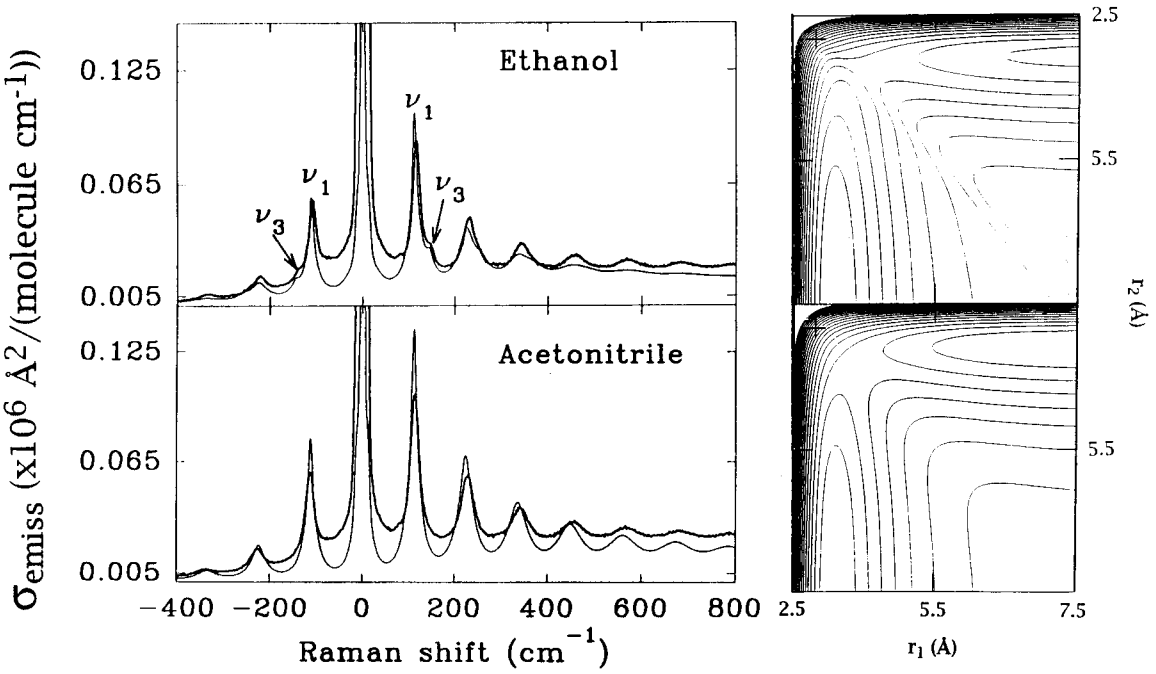

FIGURE 7. The 299 nm excited resonance Raman spectra of I_3^- in two solvents showing different intensities in the antisymmetric stretch (ν_3), and the deduced excited-state potential energy surfaces. See ref 46.

spectra (Figure 6) implies that the solvent-induced broadening in methanol has components that fluctuate on a wide range of time scales bracketing the fluorescence lifetime, perhaps related to the hydrogen-bonding dynamics in this solvent.

Symmetry Breaking in I_3^- Photodissociation. The ultrafast photodissociation of the triiodide anion, $I_3^- \rightarrow I^\bullet + I_2^-$, involves cleavage of one of two nominally equivalent I−I bonds.[42−45] In solution, solvent polarization can stabilize a localized charge distribution and induce asymmetry in the structure of the parent ion. A spectroscopic signature of such symmetry breaking is the appearance of resonance Raman intensity in the fundamental of the "antisymmetric" stretching vibration. This mode is observed with decreasing intensity in the solvent series ethanol > ethyl acetate > acetonitrile (Figure 7), indicating that the effective potential surface on which the reaction occurs is more skewed toward one set of products in ethanol than in acetonitrile. We modified a LEPS potential for the dissociative excited states to include asymmetric skewing, and calculations using this surface reproduce the data quite well.[46] Complementary femtosecond pump−probe experiments show that the dynamics of formation of the coherently vibrating I_2^- product are quite different in ethanol and acetonitrile, suggesting that the overall reaction dynamics are affected by symmetry breaking in the parent ion.[47]

Spontaneous resonance Raman has an all-time-domain analog, resonant impulsive stimulated Raman scattering (RISRS). The Fourier transform of the RISRS signal is often considered comparable to a spontaneous resonance Raman (RR) spectrum, but while equivalence has been demonstrated for nonresonant scattering,[48] the relationship between RR and RISRS is less simple due to the finite propagation time on the excited-state surface under electronically resonant conditions.[45] Our numerical simulations demonstrate that the RISRS signals tend to have smaller contributions from higher overtones and combination bands and spectral patterns that vary more strongly with excitation wavelength than do the RR spectra (Figure 8). These results help to rationalize some apparent discrepancies between our RR data and the RISRS data of Banin and Ruhman[42] on I_3^-.

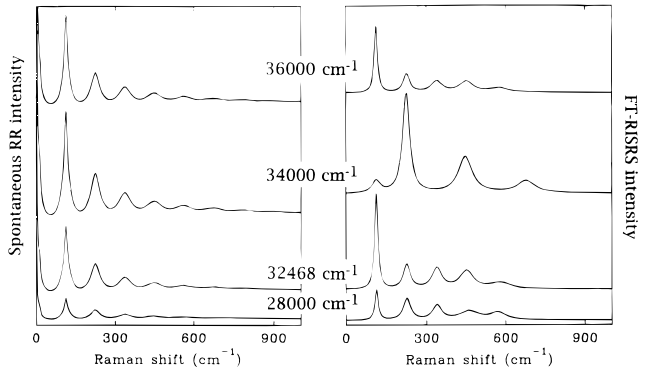

FIGURE 8. Theoretical resonance Raman spectra (assuming monochromatic excitation) and Fourier transform RISRS signals (assuming 15 fs, transform-limited pulses) for I_3^- in acetonitrile at the indicated excitation frequencies. Parameters are from ref 46, and the method of computation is described in ref. 45.

Photodissociation of Alkyl Iodides. Methyl iodide and ozone were the first small gas phase molecules whose emission spectra were analyzed by time-dependent wave packet techniques.[49] Our group has focused on using

(42) Banin, U.; Kosloff, R.; Ruhman, S. *Isr. J. Chem.* **1993**, *33*, 141−156.
(43) Banin, U.; Ruhman, S. *J. Chem. Phys.* **1993**, *98*, 4391−4403.
(44) Johnson, A. E.; Myers, A. B. *J. Chem. Phys.* **1995**, *102*, 3519−3533.
(45) Johnson, A. E.; Myers, A. B. *J. Chem. Phys.* **1996**, *104*, 2497−2507.
(46) Johnson, A. E.; Myers, A. B. *J. Phys. Chem.* **1996**, *100*, 7778−7788.
(47) Gershgoren, E.; Gordon, E.; Ruhman, S. *J. Chem. Phys.* **1997**, *106*, 4806−4809.
(48) Kinoshita, S.; Kai, Y.; Yamaguchi, M.; Yagi, T. *Phys. Rev. Lett.* **1995**, *75*, 148−151.
(49) Imre, D.; Kinsey, J. L.; Sinha, A.; Krenos, J. *J. Phys. Chem.* **1984**, *88*, 3956−3964.

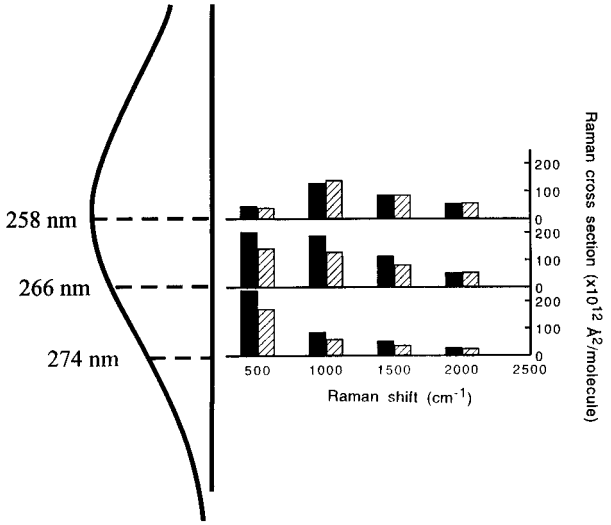

FIGURE 9. Absorption spectrum of ethyl iodide and experimental (solid) and calculated (striped) resonance Raman intensities for the C−I stretching progression. The greatly decreased intensity of the fundamental near the absorption maximum is due to resonant/preresonant interferences as discussed in ref. 50.

resonance Raman intensities to examine effects of solvation and of the alkyl substituent on the photodissociation dynamics of alkyl iodides.[50−52] The relative weakness of the directly dissociative A band transition leads to resonant/preresonant interferences that must be considered in order to analyze the intensities correctly.

Absolute resonance Raman intensities were measured for methyl iodide in hexane within the A band near 260 nm as well as between the A band and the stronger, predissociative B band near 200 nm.[52] The A band resonant spectra show a progression in the nominal C−I stretch extending to at least 16 quanta, similar to the vapor phase spectra. However, the fundamental is unexpectedly weak relative to the overtones when excited near the peak of the A band, an effect shown to arise from interference between the resonant part of the Raman amplitude and preresonant contributions from higher electronic states.[50,52,53] Such interferences are unimportant for the overtones and combination bands, which have little preresonant intensity. The intensities were simulated using an excited-state surface modeled as a harmonic, weakly displaced methyl umbrella mode and an anharmonic, directly dissociative C−I stretch, plus a preresonant contribution to the fundamental Raman intensities. The absorption spectrum and Raman excitation profiles are similar in solution and vapor phases, suggesting that the early-time dynamics of photodissociation are not strongly perturbed by solvation.

Corresponding experiments were performed on ethyl, isopropyl, and *tert*-butyl iodides.[50,54] Spectra on resonance with the A state exhibit strong overtone progressions in the C−I stretch as well as lower intensities in nominal bending and C−C stretching vibrations, indicating some

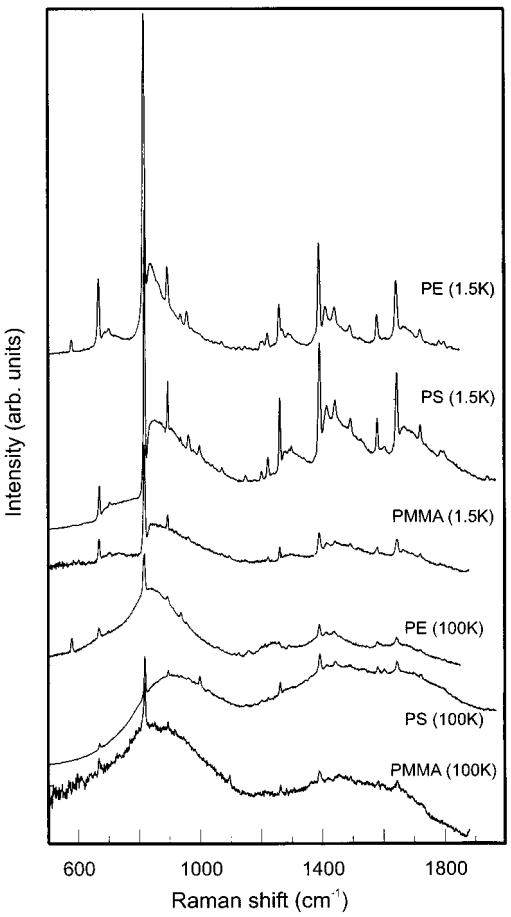

FIGURE 10. Origin-excited emission spectra of azulene in polyethylene (PE), polystyrene (PS), and poly(methylmethacrylate) (PMMA) at two different temperatures.

multidimensional character to the initial nuclear dynamics in this directly dissociative state. Resonant−preresonant interferences are also evident in these compounds (Figure 9). The absorption and resonance Raman spectra were modeled using multidimensional locally harmonic potentials to approximate the resonant surface in the Franck−Condon region, and the resulting dynamics in dimensionless normal coordinates converted to bond length and angle changes using the ground-state normal mode coefficients. This conversion is ill-defined because resonance Raman intensities (in the limit of separable vibrational dynamics) depend only on the *square* of the slope of the excited-state surface along each vibrational coordinate; the 2^n different choices of sign give 2^n different excited-state surfaces for n active vibrations. This ambiguity can be reduced by using the intensities of isotopic derivatives in which the internal coordinate composition of the ground-state normal modes is scrambled.[19,55−57] We used intensity data on the isotopically substituted compounds to choose the most consistent choice of signs and deduce the initial dynamics of nuclear motion in the dissociative state.[50,54]

Franck−Condon Activity of Intermolecular Phonons. Narrowband-excited emission spectra of molecules in low-

(50) Phillips, D. L.; Myers, A. B. *J. Chem. Phys.* **1991**, *95*, 226−243.
(51) Phillips, D. L.; Myers, A. B.; Valentini, J. J. *J. Phys. Chem.* **1992**, *96*, 2039−2044.
(52) Markel, F.; Myers, A. B. *J. Chem. Phys.* **1993**, *98*, 21−30.
(53) Galica, G. E.; Johnson, B. R.; Kinsey, J. L.; Hale, M. O. *J. Phys. Chem.* **1991**, *95*, 7994−8004.
(54) Phillips, D. L.; Myers, A. B. *J. Raman Spectrosc.* In press.
(55) Wright, P. G.; Stein, P.; Burke, J. M.; Spiro, T. G. *J. Am. Chem. Soc.* **1979**, *101*, 3531−3535.
(56) Schick, G. A.; Bocian, D. F. *J. Am. Chem. Soc.* **1984**, *106*, 1682−1694.
(57) Markham, L. M.; Mayne, L. C.; Hudson, B. S.; Zgierski, M. Z. *J. Phys. Chem.* **1993**, *97*, 10319−10325.

temperature mixed solids ("line-narrowed fluorescence") often consist of sharp, chromophore-localized vibronic lines accompanied by broader phonon sidebands.[58] The latter may be interpreted as intermolecular or matrix-localized vibrations that are Franck−Condon active in the chromophore's electronic transition. The corresponding spectra at elevated temperatures generally consist of sharp Raman-like lines superimposed on a very broad fluorescence background that presumably arises from the same extrachromophoric degrees of freedom responsible for the well-defined phonon sidebands at cryogenic temperatures. The temperature dependence of these spectra should provide insight into the coupling of solvent motions to the chromophore's electronic transition.

We have been studying the $S_1 \leftrightarrow S_0$ transition of azulene in polymer matrices. Azulene's short S_1 lifetime (a few picoseconds) makes the Raman component of the emission competitive with the broad fluorescence even near room temperature,[59] and its absorption spectrum exhibits a well-defined electronic origin. Emission spectra in several polymers (Figure 10) show the evolution from sharp zero-phonon lines with defined phonon sidebands to weaker sharp lines on a diffuse background with increasing temperature. There is no clear distinction between "Raman" and "fluorescence", so the spectra should be simulated by calculating the total emission as in eqs 6−8. We are attempting to model the temperature dependence of the spectra and determine whether the model parameters can be related to other known properties of the polymer.[60]

Conclusions

While the information obtainable through resonance Raman intensity analysis is limited, it is probably the single most useful spectroscopic technique for probing the sub-100 fs nuclear dynamics of solvated molecules. Certainly far more can be learned by combining resonance Raman with other experimental techniques, and any model for the potential energy surfaces and chromophore−environment interactions should be tested by requiring that it fit many different experimental observables.

Rapid advances in computing power and computational techniques are making it increasingly feasible to calculate directly the structures and dynamics of excited electronic states of molecules, including solvent effects. The principal application of resonance Raman and other spectroscopic information in the future may be in evaluating the results of such independent calculations, rather than attempting to derive models entirely from spectroscopy.

Work in my laboratory was performed by a number of talented graduate students and post-doctorals including Bulang Li, Xiaopei Ci, Tzyy-Schiuan Yang, Frances Markel, Kristen Kulinowski, Vinita Gupta, Mark Lilichenko, David Lee Phillips, Alan Johnson, and Dietrich Tittelbach-Helmrich and has been funded by grants from the NSF, the NIH, and the Sloan, Dreyfus, and Packard Foundations.

AR960240C

(58) Orrit, M.; Bernard, J.; Personov, R. I. *J. Phys. Chem.* **1993**, *97*, 10256−10268.
(59) Nibbering, E. T. J.; Duppen, K.; Wiersma, D. A. *J. Chem. Phys.* **1990**, *93*, 5477−5484.
(60) Renge, I. *J. Chem. Phys.* **1997**, *106*, 5835−5849.